

UDK: 676.017.5; 669.018;

## Morphological, Microstructural and Magnetic Characteristics of Electrodeposited Ni-Fe-W-Cu Alloy Powders

Miroslav Spasojević<sup>1</sup>, Siniša Randić<sup>1</sup>, Aleksa Maričić<sup>1</sup>, Tomislav Trišović<sup>2</sup>, Milica Spasojević<sup>3,\*</sup>

<sup>1</sup>Joint Laboratory for Advanced Materials of SASA, Section for Amorphous Systems, Faculty of Technical Sciences, Čačak, University of Kragujevac, Čačak, Serbia

<sup>2</sup>Institute of Technical Sciences of Serbian Academy of Science and Arts, Belgrade, Serbia

<sup>3</sup>Faculty of Chemistry, University of Belgrade, Belgrade, Serbia

---

### Abstract:

*Nanostructured Ni-Fe-W-Cu alloy powders were electrodeposited from an alkaline ammonium citrate solution on a titanium cathode. Powder particles were dendrite- and cauliflower-shaped. The dendritic particles had a high density of branches made up of interconnected globules. XRD analysis showed that the powder contained an amorphous matrix and FCC nanocrystals of the solid solution of Fe, W and Cu in Ni. As the deposition current density increased, the mean nanocrystal size decreased, and the mean value of internal microstrain and the total weight percent of Fe and Ni in the alloy increased. The powders deposited at higher current densities exhibited higher magnetization. During annealing at temperatures up to 460 °C, the powders underwent short-range ordering, which caused an increase in magnetization, whereas at temperatures above 460 °C, the magnetization decreased due to the formation of large FCC crystalline grains.*

**Keywords:** Powder; Magnetization; FCC phase; Amorphous phase; Nanomaterial.

---

### 1. Introduction

Nanostructured alloys are increasingly used in a wide range of apparatuses and devices [1-10]. Nanostructured Ni-Fe alloys have good mechanical, electrical and magnetic properties, and demonstrate high catalytic activity for a number of chemical reactions [1-10]. Alloying with small amounts of W generates nanostructured alloys exhibiting improvements in corrosion resistance, thermal stability, wear resistance, microhardness and high-temperature oxidation behavior. As the result of their good physicochemical characteristics, Ni-Fe-W alloys are in wide use for the fabrication of various components for devices such as inductor cores for electromagnets [2-4], magnetic devices [5], microwave noise filters [6], magnetic recording heads [7-9] and tunable noise suppressors [10]. They are also used in agriculture and medicine, and as catalysts in the chemical industry [11]. The metallurgical manufacture of Ni-Fe-W alloys is a highly expensive process due to high energy consumption. Therefore, much cheaper processes have been developed lately [10-25]. High quality alloys of these metals can be obtained by electrolytic deposition from environmentally friendly ammonium citrate baths. Through adjustment of the kinetic and operational

---

\*) Corresponding author: [smilica84@gmail.com](mailto:smilica84@gmail.com)

parameters of electrolysis, Ni-Fe-W alloys having specific physicochemical properties can be generated [12, 14, 19, 22, 26-33].

Annealing nanostructured materials at elevated temperatures causes changes in their microstructure, leading to changes in their physical and chemical properties [12–22, 34-36]. At temperatures below the crystallization temperature, the alloy undergoes structural relaxation, whereas amorphous phase crystallization and nanocrystalline grain growth occur at higher temperatures. These changes affect mechanical, electrical and magnetic properties, corrosion resistance, thermal stability, and catalytic activity [12-22, 34-36].

Many specifically shaped components of devices and apparatuses are manufactured from sintered powders of nanostructured Ni-Fe-W alloys. This is a simple and low-cost procedure which requires a minimum investment.

Nanostructured Ni-Fe-W alloy powders having desired characteristics cannot be produced from an ammonium citrate bath at high current efficiencies [16, 18, 21].

The deposition of these metals along with a small amount of Cu from environmentally friendly ammonium citrate solutions at high current densities and high current efficiencies can result in alloys having good mechanical, electrical and magnetic properties, and high values of corrosion resistance, thermal stability and catalytic activity, without any environmental and health risks [16, 18].

The objective of this research was to investigate the effect of current density for the deposition of Ni-Fe-W-Cu alloy powders on their morphological and microstructural characteristics and determine the correlation between these properties and magnetization.

Also, the experiment aimed to determine microstructural changes during annealing at different temperatures and the effect of these changes on magnetization.

## 2. Materials and Experimental Procedures

Nickel-iron-tungsten-copper alloys were electrodeposited on a titanium cathode, at current densities of 70–600 mA cm<sup>-2</sup> from the solution containing 0.2 mol dm<sup>-3</sup> NiSO<sub>4</sub>, 0.02 mol dm<sup>-3</sup> FeSO<sub>4</sub>, 0.04 mol dm<sup>-3</sup> Na<sub>2</sub>WO<sub>4</sub>, 0.005 mol dm<sup>-3</sup> CuSO<sub>4</sub>, 0.24 mol dm<sup>-3</sup> Na<sub>3</sub>C<sub>6</sub>H<sub>5</sub>O<sub>7</sub>, 0.8 mol dm<sup>-3</sup> NH<sub>4</sub>Cl and 0.3 mol dm<sup>-3</sup> Na<sub>2</sub>SO<sub>4</sub> at pH = 9.2±0.1 and t = 60±0.5 °C [18].

A Pektar-A-200-Varian atomic absorber was used to determine the chemical composition of the powder. Scanning electron microscopy (SEM) analysis was performed by a JEOL-JSM 5300. The particle size distribution of electrodeposited powders was determined by a Leica Q500 MC automatic device for microstructural analysis. X-ray diffraction (XRD) was recorded by a Philips PW 1710 diffractometer using CuK $\alpha$  radiation ( $\lambda$ = 0.154 nm) and a graphite monochromator. XRD data were collected with a step size of 0.03° and a collection time of 1.5 s step<sup>-1</sup>.

Magnetic measurements were performed by a modified Faraday method based on the effect of an inhomogeneous magnetic field on the powder. The magnetic field strength of the powder was 10 kA m<sup>-1</sup>. Magnetic force measurements were carried out with a sensitivity of 10<sup>-6</sup> N in an argon atmosphere.

## 3. Results and Discussion

Black Ni-Fe-W-Cu alloy powders were obtained on the titanium cathode from an ammonium citrate bath at current densities of 70–600 mA cm<sup>-2</sup>. The chemical composition of the powders was found to depend on deposition current density (Table I).

As shown by SEM micrographs, deposition at all current densities resulted in cauliflower-shaped and dendritic particles (Figs. 1 and 2, respectively). The dendrites exhibited a high density of secondary and higher-order branches made up of a series of

interconnected globules [18]. During further deposition, the dendrites were transformed into cauliflowers. However, some dendrites, before the completion of their transformation into cauliflowers, became detached from the cathode surface and fell onto the bottom of the electrochemical cell.

**Tab. I** Chemical composition of powders.

$j$ ( $\text{mA cm}^{-2}$ )	Composition
70	$\text{Ni}_{86.70}\text{Fe}_{5.66}\text{W}_{0.74}\text{Cu}_{6.90}$
200	$\text{Ni}_{86.30}\text{Fe}_{8.27}\text{W}_{1.03}\text{Cu}_{4.40}$
400	$\text{Ni}_{86.00}\text{Fe}_{9.80}\text{W}_{1.30}\text{Cu}_{2.90}$
600	$\text{Ni}_{85.77}\text{Fe}_{10.63}\text{W}_{1.40}\text{Cu}_{2.20}$

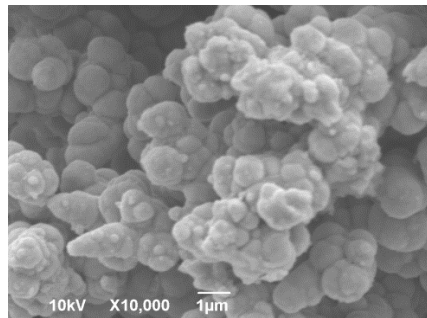


**Fig. 1.** SEM micrographs of Ni-Fe-W-Cu alloy electrodeposited at a current density of  $j = 70 \text{ mA cm}^{-2}$ .

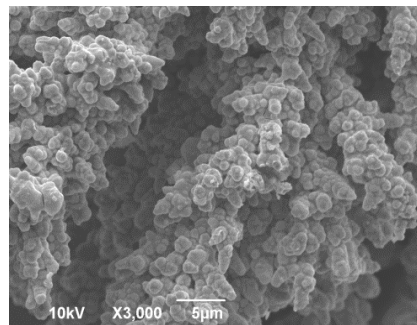


**Fig. 2.** SEM micrographs of Ni-Fe-W-Cu alloys electrodeposited at a current density of  $j = 70 \text{ mA cm}^{-2}$ .

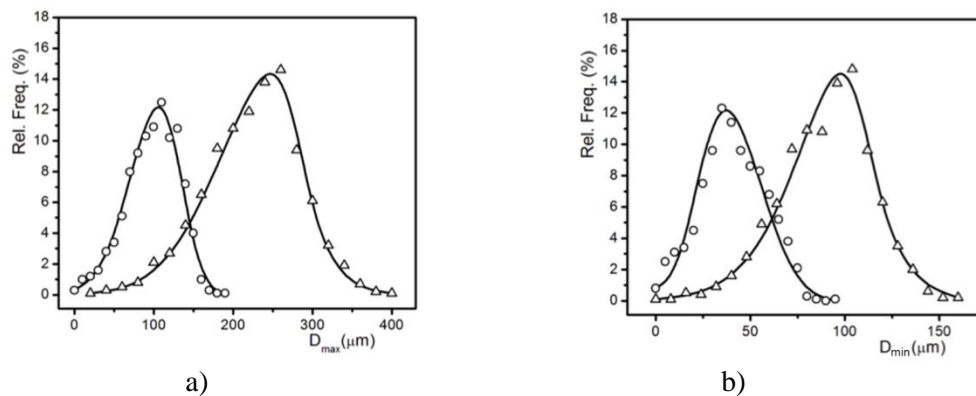


**Fig. 3.** Relative frequency distribution of: a) maximum,  $D_{\text{max}}$ , and b) minimum,  $D_{\text{min}}$ , particle size of alloy powder: obtained at  $\Delta - j = 70 \text{ mA cm}^{-2}$  and  $\circ - j = 600 \text{ mA cm}^{-2}$ .

The size and shape of electrodeposited particles were dependent on current density. The average particle size decreased and particle roundness increased with increasing deposition current density (Fig. 3).

The phase structure of the powders was determined by XRD analysis (Fig. 4). The XRD patterns showed that all powders deposited at current densities of 70-600 mA cm<sup>-2</sup> consisted of an amorphous matrix and FCC nanocrystals of the solid solution of Fe, W and Cu in Ni.

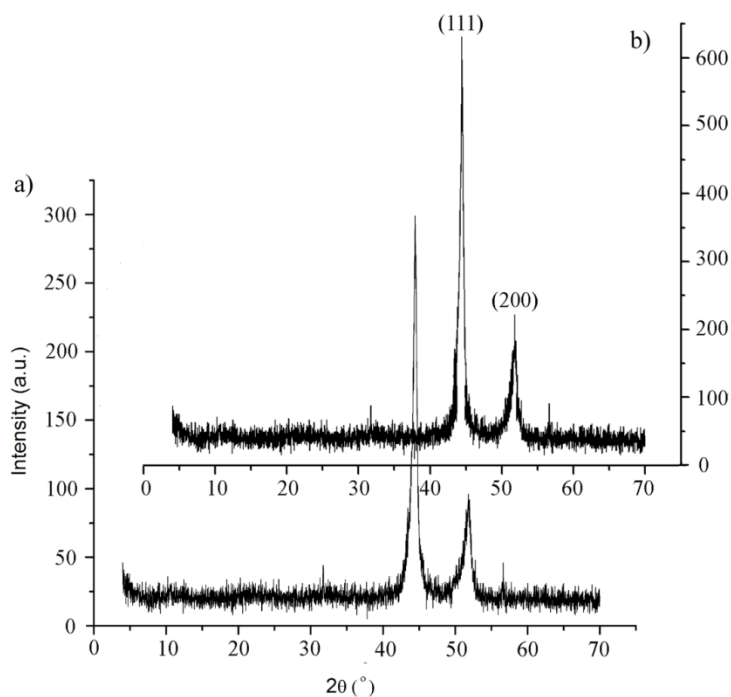


**Fig. 4.** XRD pattern for Ni<sub>86.00</sub>Fe<sub>9.80</sub>W<sub>1.30</sub>Cu<sub>2.90</sub> obtained at 400 mA cm<sup>-2</sup>: a) – as-deposited and b) annealed for 60 minutes at 600°C

As revealed by XRD analysis, the mean nanocrystal size decreased, and internal microstrain and amorphous phase content increased with increasing deposition current density [17, 18]. As the deposition current density increased, the cathodic polarization increased, leading to a decrease in the critical radius of the nucleus and, hence, an increase in nucleation rate, and the formation of small nanocrystals exhibiting high internal microstrain.

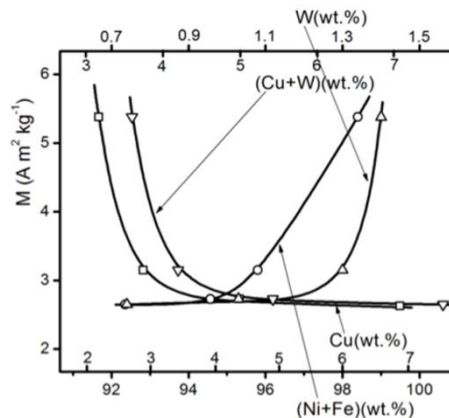
**Tab. II** Magnetization of as-deposited Ni-Fe-W-Cu alloy powders at 20 °C.

Alloy	Magnetization (A m <sup>2</sup> kg <sup>-1</sup> )
Ni <sub>86.70</sub> Fe <sub>5.66</sub> W <sub>0.74</sub> Cu <sub>6.90</sub>	2.65
Ni <sub>86.30</sub> Fe <sub>8.27</sub> W <sub>1.03</sub> Cu <sub>4.40</sub>	2.73
Ni <sub>86.00</sub> Fe <sub>9.80</sub> W <sub>1.30</sub> Cu <sub>2.90</sub>	3.15
Ni <sub>85.77</sub> Fe <sub>10.63</sub> W <sub>1.40</sub> Cu <sub>2.20</sub>	5.38

Also, higher rates of nucleation and the formation of small nanocrystals were indirectly facilitated by the presence of Fe, Cu and W in the FCC Ni solid solution. These

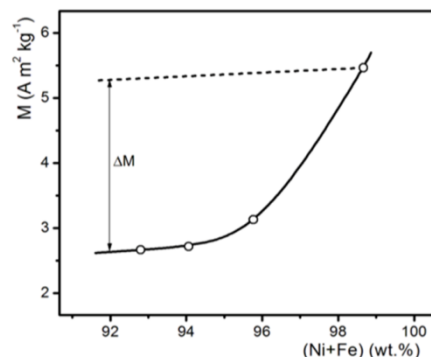
atoms deformed the crystal lattice and, thus, slowed down the growth of nanocrystals, thereby leading to favorable conditions for faster nucleation. Tungsten atoms were the largest and, therefore, their effect was the most pronounced. Copper was deposited from the solution containing complex ions under the diffusion-limiting current at high overpotentials. Therefore, copper deposition enabled a considerably higher rate of nucleation and the formation of powder deposits [16, 18].

The magnetic properties of electrodeposited Ni-Fe-W-Cu alloy powders were dependent on their chemical composition and microstructure. Table II. shows the magnetization of as-deposited alloy powders at 20 °C as a function of chemical composition.



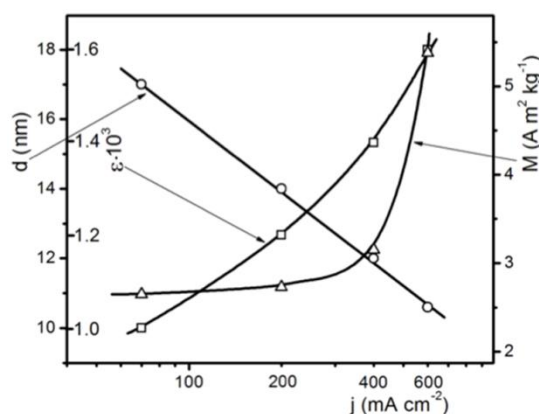
**Fig. 5.** Magnetization,  $M$ , at 20 °C, as a function of:  $\square$  – Cu content;  $\Delta$  – W content; and the sum of:  $\circ$  – Ni+Fe, and  $\nabla$  – Cu+W contents

Figure 5. presents the dependence of magnetization,  $M$ , on: a) – Cu content; b) – W content; and the sum of the contents of: c) – Ni+Fe, and d) – Cu+W. The diagrams show magnetization as a complex function of the contents of these metals in the alloy, which increases with increasing sum of Ni+Fe contents, and decreases with increasing sum of Cu+W contents. If the contents of these metals decreased in the alloy containing 98.4 wt.% (Ni+Fe) while the microstructure remained unchanged, the magnetization would decrease along the dashed line. Figure 6. shows that magnetization decreased at a considerably higher rate with decreasing Ni+Fe content, indicating a considerably greater decrease in magnetization,  $\Delta M$ , due to microstructural changes.



**Fig. 6.** Magnetization as a function of the sum of Ni+Fe contents (solid line), and hypothetical dependence of magnetization upon the sum of Ni+Fe contents if the microstructure at any composition were identical to that of the alloy containing 98.4 wt.% (Ni+Fe) (dashed line)

Figure 7. presents magnetization, mean nanocrystal size and mean internal microstrain values as a function of electrodeposition current density. The dependences obtained indicate that current density had a significant effect on microstructure i.e. nanocrystalline grain size and internal microstrain intensity, and hence on magnetization. As shown, the magnetization was considerably enhanced as the mean nanocrystalline grain size decreased from 17.0 nm to 10.6 nm.



**Fig. 7.** Magnetization,  $M$ , mean nanocrystal size,  $d$ , and mean internal microstrain values,  $\epsilon$ , as a function of electrodeposition current density.

Deposition current density has both a direct and an indirect effect on alloy microstructure [12-20, 22, 26,]. The direct effect is due to an increase in cathodic polarization with increasing current density [15, 17, 20, 21,]. The increase in polarization causes a decrease in the critical radius of the nucleus, a reduction in the number of atoms in the critical nucleus, and a decrease in the induction period. The number of atoms in the critical nucleus of a metal decreases with the square of the deposition overpotential for the metal. These facts indicate that the increase in current density causes an increase in the rate of nucleation. The formation of new nuclei prevents the growth of existing crystals. Therefore, small crystalline grains are obtained during deposition at high current densities. During a slow deposition process, at low current densities, it is easier for adatoms of metals to build more ordered crystal structures which exhibit a lower density of chaotically distributed dislocations and lower internal microstrain. At high deposition densities, small grains are obtained, with a thick less ordered layer making up the amorphous phase existing between them [17, 19, 26, 37]. Therefore, electrodeposition does not result in an ideal amorphous phase with a completely randomized distribution of spacings between neighboring atoms; rather, it leads to the formation of a phase exhibiting any degree of short-range order [38, 39]. The higher the deposition current density, the greater the disorder. Transmission electron microscopy showed that Ni-Fe-W alloy with the mean crystalline grain size below 15 nm contained an amorphous matrix, in addition to the FCC phase. Moreover, the smaller the crystalline grains, the greater the amorphous phase content [17, 18].

The indirect effect of deposition current density is expressed through the presence of Fe, W and Cu in the FCC nickel solid solution. Atoms of these metals cause the deformation of the crystal lattice of nickel. Their presence causes an increase in the mean interatomic distance in the FCC phase, as recorded by the shift of (111) and (200) plane peak maxima to lower  $2\theta$  values. [12-20, 22, 26]. Tungsten atoms are considerably greater than Ni atoms and, hence, their presence causes the largest deformation in the crystal lattice. The newly arrived adatoms are difficult to embed into the deformed lattice [12-20, 22, 26]. This favors the formation of new nuclei which, then, prevent further growth of existing nuclei. The above considerations show that, in multicomponent deposits, deposition current density has a very

complex effect on the chemical composition and microstructure of deposits and, hence, their magnetic properties [15, 21, 29, 30, 33].

As presented in Figure 7, magnetization decreased with increasing mean crystalline grain size. Large crystalline grains hampered the orientation of some magnetic domains and reduced the shift of oriented domain walls towards expansion [15, 21, 29, 30, 33]. These phenomena gave rise to an increase in magnetization as the crystalline grain size decreased. However, this increase took place only up to a critical size of the grain.

Magnetization decreased during a further reduction in crystalline grain size. This decrease was caused by the increased proportion of the amorphous phase, which exhibited considerably lower magnetization, to the detriment of the decrease in the content of the FCC phase, which exhibited considerably higher magnetization. These considerations show the need to establish an optimum deposition current density for the obtainment of deposits with the crystalline grain size ensuring maximum magnetization.

Annealing as-deposited powders at elevated temperatures induces changes in their microstructure and, hence, their magnetic properties [15, 21, 29, 30, 33].

XRD analysis was used to monitor the effect of annealing temperature on the phase structure of powders. Magnetic properties were assessed by measuring magnetization during annealing at elevated temperatures as well as by measuring the magnetization of powders cooled at 20 °C after annealing.

Powders were heated at a rate of 20 °C min<sup>-1</sup> up to a temperature (limiting temperature), and their magnetization was concurrently measured. Then, they were cooled at 20 °C, and reheated at the same rate to a higher temperature. Seven successive heating and cooling cycles were conducted. Each successive heating was performed up to a higher limiting temperature. Table III presents limiting heating temperature as a function of the number of thermal cycles and deposition current density for the powder.

**Tab. III** Dependence of limiting heating temperature upon the number of thermal cycles.

	Current density (mA cm <sup>-2</sup> )			
	70	200	400	600
Number of thermal cycles	Limiting temperature (°C)			
1	180	170	160	150
2	260	240	220	240
3	380	320	360	360
4	420	420	420	420
5	460	460	460	460
6	485	485	485	540
7	600	600	600	600

For easy reference, Figures 8a, 8b, 8c and 8d present only the curves for the first, sixth and seventh thermal cycle.

The diagrams presented in Figure 8 show that, during heating of as-deposited powders obtained at different current densities, in the temperature range of 20 °C to  $t_s$  ( $t_s$  = stability temperature), the magnetization of powders does not change. This indicates that no structural change takes place in as-deposited powders during annealing in this temperature range. The temperature  $t_s$  is dependent on deposition current density (Figs. 8 and 9). As the current density increases, the stability temperature,  $t_s$ , of as-deposited powders decreases, as illustrated in Table IV.

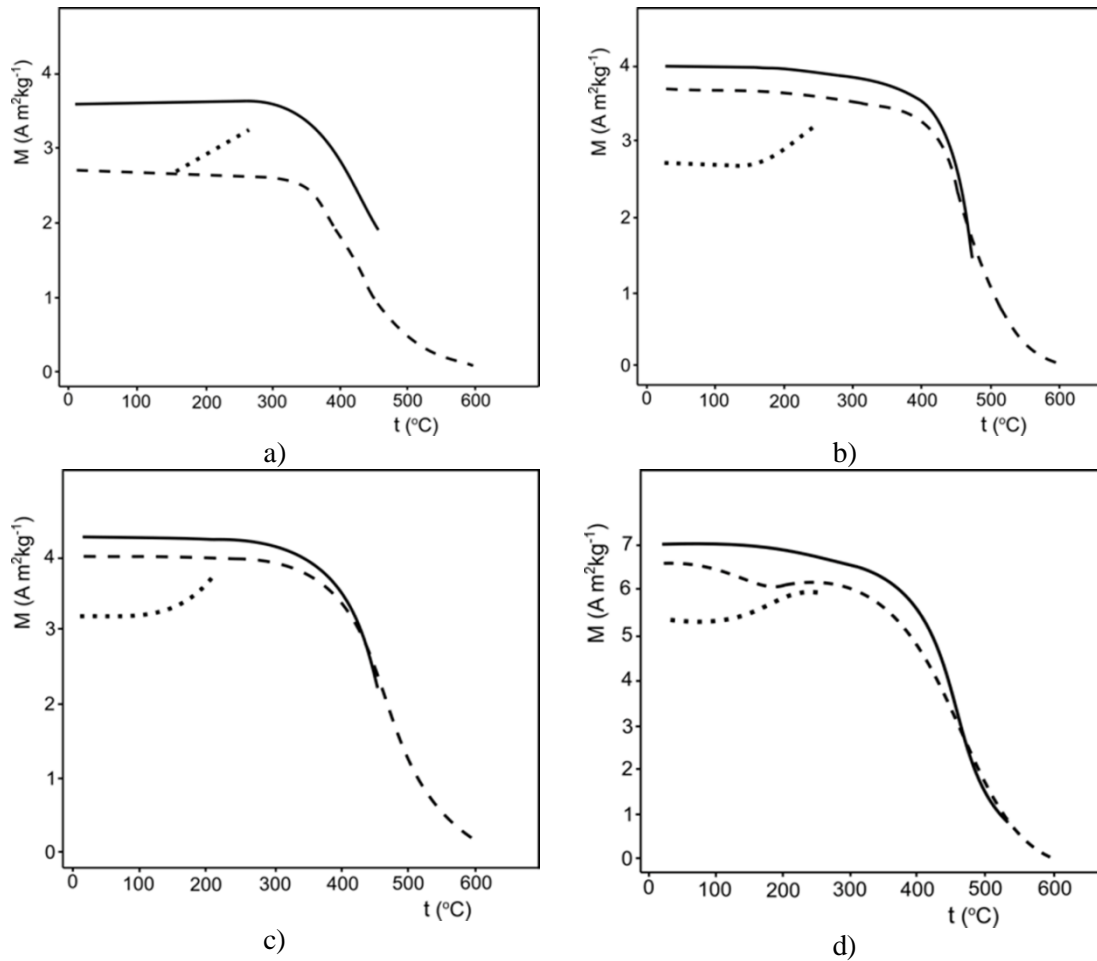


**Fig. 8.** Magnetization as a function of temperature. Heating rate 20°C min<sup>-1</sup>. a) (···) - second heating up to 260 °C, (---) - sixth heating up to 485 °C and (—) - seventh heating up to 600 °C; b) (···) - second heating up to 240 °C, (---) - sixth heating up to 485 °C and (—) - seventh heating up to 600°C; c) (···) - second heating up to 220°C, (---) - sixth heating up to 485 °C and (—) - seventh heating up to 600 °C; d) (···) - second heating up to 240 °C, (---) - sixth heating up to 540 °C and (—) - seventh heating up to 600°C. Powders were obtained at: a) - 70 mA cm<sup>-2</sup>, b) - 200 mA cm<sup>-2</sup>, c) - 400 mA cm<sup>-2</sup> and d) - 600 mA cm<sup>-2</sup>.

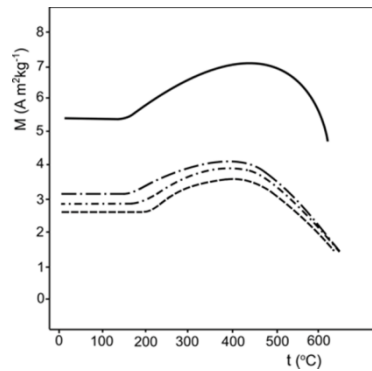


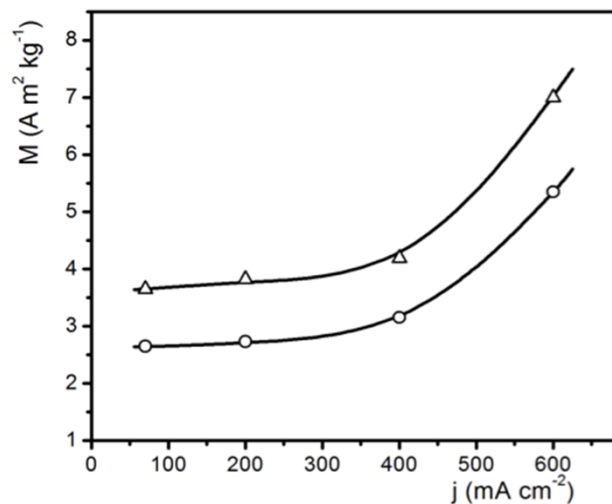
**Fig. 9.** Magnetization of powders cooled to 20°C as a function of the limiting temperature of the previous annealing cycle. The powders were obtained at current densities: (---) - 70 mA cm<sup>-2</sup>; (- · -) - 200 mA cm<sup>-2</sup>; (- - -) - 400 mA cm<sup>-2</sup>, and (—) - 600 mA cm<sup>-2</sup>.

**Tab. IV** Stability temperature as a function of current density for powder deposition.

$j$ ( $\text{mA cm}^{-2}$ )	70	200	400	600
$t_s$ ( $^{\circ}\text{C}$ )	180	170	160	150

The powders obtained at increased current densities showed greater instability as they contained small crystalline grains which exhibited a higher density of chaotically distributed dislocations and higher internal microstrain values. Therefore, at low temperatures, these powders were subjected to structural relaxation. During heating of as-deposited powders in the temperature range of  $t_s$  to 360  $^{\circ}\text{C}$ , magnetization increased with increasing temperature. During further heating, at temperatures between 360 and 400  $^{\circ}\text{C}$ , there was a gradual decline in magnetization, as opposed to its abrupt decrease at temperatures from 400 to 500 $^{\circ}\text{C}$ . In the temperature range of 500 to 600  $^{\circ}\text{C}$ , magnetization decreased slowly again. The diagrams in Figure 9 show that the powders obtained at different current densities have the same Curie temperature of 600  $^{\circ}\text{C}$ . The decrease in the magnetization of heated powders, in the temperature range of 360-600  $^{\circ}\text{C}$ , as induced by increasing temperature, is the result of magnetic domain reorientation due to the effect of heat.

The plots of the magnetization of powders cooled at 20  $^{\circ}\text{C}$  as a function of limiting annealing temperature (Fig. 8) show that the magnetization of the cooled samples increased with the increase in annealing temperature from  $t_s$  to 460  $^{\circ}\text{C}$ . The XRD patterns of powders previously annealed in this temperature range were congruous with those of as-deposited powders. This congruity indicated that, during the annealing of as-deposited powders in the temperature range  $t_s$ -460  $^{\circ}\text{C}$ , neither amorphous phase crystallization nor growth of large grains to the detriment of small ones occurred in the alloys. The increase in the magnetization of samples annealed at temperatures between  $t_s$  and 460  $^{\circ}\text{C}$  and, then, cooled at 20  $^{\circ}\text{C}$  is due to structural relaxation [15, 21, 29, 30, 33].

**Fig. 10.** Magnetization of  $\circ$  - as-deposited powders, and  $\Delta$  - powders pre-annealed at 460  $^{\circ}\text{C}$ , cooled at 20  $^{\circ}\text{C}$ , as a function of deposition current density.

Electrodeposition did not yield an ideal FCC structure of the solid solution of Fe, W and Cu in Ni; it led to a structure exhibiting defects in the crystal lattice. Neither did electrodeposition result in an ideal amorphous phase with a completely randomized distribution of spacings between adjacent atoms; it produced a structure exhibiting a small or large degree of short-range ordering [38, 39]. Disorders in both the FCC crystal phase and the amorphous matrix were larger in the deposits formed at high current densities. During the

annealing of Ni-Fe-W-Cu electrodeposits, in the temperature range of  $t_s$  to 460 °C, short-range ordering occurred in both the FCC crystal phase and the amorphous matrix through the effect of heat. In this temperature range, as the result of heat, some atoms at high energy levels cross the energy barrier and settle at lower energy levels. Spacings between the atoms arriving at lower levels and adjacent atoms are small, and therefore their external orbitals overlap to a large degree with the orbitals of surrounding atoms of the same type and symmetry. This increases the exchange integral and the electron density of states near the Fermi level, and makes it easier for these atoms to adjoin energetically favorable magnetic domains [15, 21, 29, 30, 33].

The lower density of chaotically distributed dislocations, resulting from short-range ordering, ensures greater mobility of magnetic domain walls i.e. their expansion, and facilitates the orientation of these domains in the external magnetic field, thus leading to an increase in magnetization [15, 21, 29, 30, 33].

Figure 10 presents the magnetization of a) as-deposited powders, and b) powders pre-annealed at 460 °C, cooled at 20 °C, as a function of deposition current density. The diagrams presented show the highest increase in magnetization during short-range ordering in the powder electrodeposited at the highest current density (600 mA cm<sup>-2</sup>).

The diagrams presented in Figure 8 show that, after annealing at temperatures above 460 °C, the magnetization of samples cooled at 20 °C decreased with increasing annealing temperature. Annealing resulted in microstructural changes, which affected the magnetization of powders, i.e. the crystallization of the amorphous phase (magnetization was lower than that of the small-grained nanocrystalline phase and higher than that of the large-grained nanocrystalline phase), growth of large crystalline grains (exhibiting lower magnetization) to the detriment of small nanocrystals (showing higher magnetization), a decrease in internal microstrain, as well as in the density of chaotically distributed dislocations, accompanied by an increase in magnetization. All these changes combined caused a decrease in magnetization, thus indicating that the magnetization during annealing at temperatures above 460 °C was dominantly affected by the formation of large FCC crystals of the solid solution of Fe, W and Cu in Ni. Large crystalline grains mostly hamper or prevent the orientation of magnetic domains in the external magnetic field [15, 21, 29, 30, 33]. Large crystalline grains also reduce magnetic wall mobility, thereby preventing the growth (increase) of domains [15, 21, 29, 30, 33].

The formation of large FCC crystalline grains of the solid solution of Ni, Fe, W and Cu was confirmed by the XRD patterns of alloys cooled at 20 °C after annealing at 600 °C (Fig.4a and 4b).

XRD analysis showed that, compared to the XRD patterns of unannealed alloys, the XRD patterns of annealed alloys had higher peak intensity and smaller peak width at half-height, and higher values of the relative peak intensity integrals.

The highest magnetization was in the Ni<sub>85.8</sub>Fe<sub>10.6</sub>W<sub>1.4</sub>Cu<sub>2.2</sub> alloy obtained at a current density of 600 mA cm<sup>-2</sup> and annealed at 460 °C. All alloys electrodeposited from an ammonium citrate solution in the current density range of 70 to 600 mA cm<sup>-2</sup> and annealed at 460 °C were magnetically stable up to 360 °C, and structurally stable up to 460 °C.

#### 4. Conclusion

Nickel-iron-tungsten-copper alloy powders were deposited from an ammonium citrate bath on a titanium cathode at current densities ranging between 70 and 600 mA cm<sup>-2</sup>.

Powder particles are dendrite- and cauliflower-shaped. The dendrites have a large density of secondary and higher-order branches made up of a series of interconnected globules. At high current densities, small rounded particles exhibiting a higher density of branches are formed.

Powders contain an amorphous matrix with embedded FCC nanocrystals of the solid solution of Fe, W and Cu in Ni. At high current densities, the resulting powder has a higher proportion of the amorphous phase and smaller nanocrystals exhibiting higher internal microstrain.

The magnetization of the electrodeposited Ni-Fe-W-Cu alloy powders is dependent upon their chemical composition and microstructure. As the deposition current density increased, the total weight percent of Fe and Ni increased, the mean nanocrystal size decreased, and internal microstrain and the mean density of chaotically distributed dislocations increased, which caused an increase in magnetization. During annealing at temperatures up to 460 °C, the powders underwent structural relaxation, which caused an increase in magnetization. At temperatures above 460 °C, FCC crystalline grains of the solid solution of Fe, W and Cu grew to the detriment of small crystals and the amorphous matrix. Large crystal grains prevented the orientation of some magnetic domains and reduced the mobility of walls of other domains towards expansion, thus inducing a decrease in magnetization. Ni-Fe-W-Cu alloy powders electrodeposited from an ammonium citrate solution at current densities of 70 to 460 mA cm<sup>-2</sup> and annealed at 460 °C are magnetically stable up to 360 °C, and structurally stable up to 460 °C.

## Acknowledgments

This study was financially supported by the Ministry of Education and Science of the Republic of Serbia through Project Ref. No. 172057.

## 5. References

1. S. Steeb and H. Warlimont, *Rapidly Quenched Metals*, Elsevier, Amsterdam (1985).
2. T. O'Donnell, N. Wang, S. Kulkarni, R. Meere, F.M.F. Rhen, S. Roy, and S.C. O'Mathuna, *J. Magn. Mater.*, 322 (2010) 1690.
3. E. Kubo, N. Ooi, H. Aoki, D. Watanabe, J.H. Jeong, C. Kimura, and T. Sugino, *Jpn. J. Appl. Phys.*, 49 (2010) 04DB17.
4. T. Dastagir, W. Xu, S. Sinha, H. Wu, Y. Cao, and H. Yu, *Appl. Phys. Lett.*, 97 (2010), 162506.
5. O. Song, C. A. Ballentine, and R. C. O'Handley, *Appl. Phys. Lett.*, 64 (1994) 2593.
6. C. Jiang, D. Xue, and W. Sui, *Thin Solid Films*, 519 (2011) 2527.
7. E. I. Cooper, C. Bonhote, J. Heidmann, Y. Hsu, P. Kern, J. W. Lam, M. Ramasubramanian, N. Robertson, L. T. Romankiw, and H. Xu, *IBM J. Res. Dev.*, 49 (2005) 103.
8. B. Koo and B. Yoo, *Surf. Coat. Tech.*, 205 (2010) 740.
9. T. Osaka, T. Asahi, J. Kawaji, and T. Yokoshima, *Electrochim. Acta*, 50, 4576 (2005).
10. B.K. Kuanr, R. Marson, S.R. Mishra, A.V. Kuanr, R. E. Camley, and Z. J. Celinski, *J. Appl. Phys.*, 105 (2009) 07A520.
11. M. A. Oliver-Tolentino, E.M. Arce-Estrada, C.A. Cortés-Escobedo, A.M. Bolarín-Miro, F. Sánchez-De Jesús, R. de G. González-Huerta, and A. Manzo-Robledo, *J. Alloys Comp.*, 536 (2012) S245.
12. M. Donten, H. Cesiulis, and Z. Stojek, *Electrochim. Acta*, 45 (2000) 3389.
13. S.J. Mun, M. Kim, T.H. Yim, J.H. Lee, and T. Kang, *J. Electrochem. Soc.*, 157 (2010) D177.
14. F. He, J. Yang, T. Lei, and C. Gu, *Appl. Surf. Sci.*, 253 (2007) 7591.
15. M. Spasojević, N. Ćirović, L. Ribić-Zelenović, P. Spasojević, and A. Maričić, *J. Electrochem. Soc.*, 161 (2014) D463.

16. Z. Vuković, P. Spasojević, M. Plazinić, J. Živanić, and M. Spasojević, J. Optoelectron. Adv. M., 16 (2014) 985.
17. N. Ćirović, P. Spasojević, L. Ribić-Zelenović, P. Mašković, and M. Spasojević, Sci. Sinter., 47 (2015) 347.
18. M. Spasojević, D. Gospavić, and M. Spasojević, J. Electrochem. Soc., 163 (2016) D842.
19. K. R. Sriraman, S. Ganesh Sundara Raman and S. K. Seshadri, Mater. Sci. Tech., 22 (2006) 14.
20. L. Ribić-Zelenović, N. Ćirović, M. Spasojević, N. Mitrović, A. Maričić, and V. Pavlović, Mater. Chem. Phys., 135 (2012) 212.
21. M. Spasojević, L. Ribić-Zelenović, A. Maričić, and P. Spasojević, Powd. Tech., 254 (2014) 439.
22. P. Esther, C. Joseph Kennady, P. Saravanan, and T. Venkatachalam, J. Non-Oxide Glasses, 1 (2009) 301.
23. S.H. Hong and H.J. Ryu, Mater. Sci. Eng: A, 344 (2003) 253.
24. Z.W. Zhang, J.E. Zhou, S.Q. Xi, G. Ran, and P.L. Li, Mater. Sci. Eng: A, 379 (2004) 148.
25. Z.W. Zhang, J.E. Zhou, S.Q. Xi, G. Ran, P.L. Li, and W.X. Zhang, J. Alloys Compd., 370 (2004) 186.
26. K.R. Sriraman, S. Ganesh Sundara Raman, and S.K. Seshadri, Mater. Sci. Eng: A, 418 (2006) 303.
27. Milica Spasojević, D. Marković, M. Spasojević, Z. Vuković, A. Maričić and L. Ribić-Zelenović, Sci. Sinter., 51(2019) 209-221.
28. L. Ribić-Zelenović, M. Spasojević, and A. Maričić, Mater. Chem. Phys., 115 (2009) 347.
29. L. Ribić-Zelenović, M. Spasojević, A. Maričić, and M.M. Ristić, Sci. Sinter., 41 (2009) 175.
30. N. Ćirović, P. Spasojević, L. Ribić-Zelenović, P. Mašković, A. Maričić, and M. Spasojević, Sci. Sinter., 48 (2016) 1.
31. A. Maričić, M. Spasojević, L. Rafailović, V. Milovanović, and L. Ribić-Zelenović, Mater. Sci. Forum, 453 (2004) 411.
32. L. Ribić-Zelenović, L. Rafailović, M. Spasojević, and A. Maričić, Phy. B, 403 (2008) 2148.
33. O. Younes and E. Gileadi, Electrochem. Solid-State Lett., 3 (2000) 543.
34. M. Spasojević, L. Ribić-Zelenović, N. Ćirović, P. Spasojević, and A. Maričić, Sci. Sinter., 44 (2012) 197.
35. I. Milićević, Milica Spasojević, R. Savković, M. Spasojević, A. Maričić, Sci. Sinter., 50 (2018) 421.
36. J. Chaurasia, M. Ayyapan, P. Patel, R. A. A. Rajan, Sci. Sinter., 49, (2017) 445.
37. T. Yamasaki, Scripta Mater., 44 (2001) 1497.
38. K. E. Heusler and D. Huerta, J. Electrochem. Soc., 136 (1989) 65.
39. M. Donten, J Solid State Electrochem., 3 (1999) 87.

---

**Сажетак:** Из алкалног амонијачно-цитратног раствора електродепоновани су на титанској катоди наноструктурни прахови Ni, Fe, W и Cu. Честице прахова имале су облике дендрита и карфиола. Дендрити су имали велику густину грана сатканих од међусобно повезаних глобула. XRD анализом установљено је да су се прахови састојали од аморфне матрице и нанокристала FCC фазе чврстог раствора Fe, W и Cu у Ni. Са порастом густине струје депозиције опада средња димензија нанокристала а расте средња вредност унутрашњих микронапрезања и удео збира масе Fe и Ni у легурама. Прахови депоновани на већим густинама струје имају већу магнетизацију. У праховима се током одгревања до 460°C одвија уређење структуре на кратко што

---

узрокује повећање магнетизације, док на температурама већим од 460 °C магнетизација опада услед формирања већих кристалних зрна FCC фазе.

**Кључне речи:** прах, магнетизација, FCC фаза, аморфна фаза, наноматеријали.

---

© 2020 Authors. Published by association for ETRAN Society. This article is an open access article distributed under the terms and conditions of the Creative Commons — Attribution 4.0 International license (<https://creativecommons.org/licenses/by/4.0/>).

